Mass spectroscopy study of products from exposure of cyclotrimethylene-trinitramine single crystals to KrF excimer laser radiation

Cite as: Journal of Applied Physics **67**, 3641 (1990); https://doi.org/10.1063/1.345318
Submitted: 25 September 1989 . Accepted: 03 January 1990 . Published Online: 17 August 1998

J. T. Dickinson, L. C. Jensen, D. L. Doering, and R. Yee

Mass spectroscopy study of products from exposure of cyclotrimethylene-trinitramine single crystals to KrF excimer laser radiation

J. T. Dickinson, L. C. Jensen, D. L. Doering,[a] and R. Yee[b]
Department of Physics, Washington State University, Pullman, Washington 99164-2814

(Received 25 September 1989; accepted for publication 3 January 1990)

We report mass spectroscopic measurements of the charged particle, neutral, and excited neutral species emitted from the irradiation of single-crystal cyclotrimethylene-trinitramine (RDX) with 248-nm, 20-ns laser pulses. At laser fluences above 5 mJ/cm^2 we observe RDX decomposition products of relatively small mass in both neutral and ionic states. With increasing fluence we see clear etching of the crystal, an increase in kinetic energy of the products, and the appearance of an intense, excited neutral species which we identify as NO in an energetic, long-lived electronic excited state. Evidence is also presented for a sustained decomposition reaction ignited by the laser pulse.

I. INTRODUCTION

When absorbing materials are subjected to relatively intense, short-wavelength laser radiation, processes categorized as *photochemical* and *photothermal* can occur which result in the ejection of atomic and molecular fragments from the surface. When such removal of material is significant, resulting in measurable localized "etching" of the surface, it is referred to as photoablation.[1] Explosive molecular crystals tend to absorb radiation in the ultraviolet[2] with potential for initiating photodecomposition reactions in the near-surface region. Laser bombardment of explosive crytals has been previously reported. Yang and Menichelli[3] used a *Q*-switched ruby laser to detonate pentaerythritol tetranitrate (PETN), cyclotrimethylene-trinitramine (RDX), and tetryl utilizing the shock wave produced by strong light absorption in a metal film. Tang *et al.*[4] have examined decomposition of explosives by analysis of the $\pm$ ion products from 266-nm, 5-ns laser pulses on RDX, PETN, AgN_3, and $Pb(N_3)_2$ using laser ionization mass analysis (LIMA). These workers reported rapid (but not self-sustained) decomposition of RDX and PETN and for low fluences, the decomposition of the azides. At higher fluences, the azides detonated under laser bombardment. For RDX, Tang *et al.*[4] saw both positive- and negative-ion masses ranging from 16–176 amu. A number of ionic species observed in this study coincide in mass with several of the decomposition products observed by Zhao, Hintsa, and Lee[5] in gas-phase infrared multiphoton dissociation of RDX. Also, there has been evidence presented[6] of uv sensitization of liquid nitromethane due to creation of a nitromethane aci ion ($CH_2NO_2^-$).

In this work, we report on the consequences of bombarding single crystals of RDX with pulses of excimer laser light at 248 nm. We show that at laser fluences above 5 mJ/cm^2 we observe RDX decomposition products of relatively small mass in both neutral and $\pm$ ionic states, as well as photoelectrons. With increasing fluence we see clear etching of the crystal, an increase in kinetic energy of the products, and the appearance of an intense, long-lived excited neutral species. We identify this excited neutral as NO in a metastable electronic state. We present evidence of both thermal and nonthermal processes involved in creating the observed products along with their observed energy distributions. We also present evidence of a sustained decomposition reaction which continues for many microseconds following the laser pulse.

II. EXPERIMENT

Single crystals of high optical quality RDX were grown from an acetone solution in dimensions of approximately 1 cm in length and a few mm in thickness. Prior to mounting, the crystals were cleaved in air which generally exposes [001] surfaces.[7,8] RDX has an orthorhombic structure (space group *Pbca*) with $a = 1.308$ nm, $b = 1.157$ nm, $c = 1.071$ nm, and $z = 8$.[9] The samples were mounted on a translatable stage in a vacuum chamber maintained at a pressure of 10^{-5} Pa or less. The laser beam was directed through a quartz window at an angle of about 20° to the sample surface normal.

The radiation source was a Lambda Physik Model EMG 203 excimer laser, which produced 20-ns pulses of 248-nm radiation (KrF). The laser energy/pulse was measured with a Gentec ED 500 joule meter. The laser beam was focused by a lens of 1-m focal length to produce a 0.5×1 mm^2 rectangular spot on the sample surface with a maximum fluence of 5 J/cm^2. Neutral density filters were used to reduce the fluence by calibrated amounts. Optical microscopy of the ablated surfaces demonstrated that the beam was generaly uniform in the central portion, but showed some irregularities on the edges due to slight misalignment of the optical components.

Time-of-flight (TOF) measurements of ions and excited neutral particles were made with a Chenneltron electron multiplier (CEM), Galileo Electro-Optics Model 4821. Excited neutrals can be detected when their internal energy is sufficient to cause Auger de-excitation (e.g., metastable atoms and molecules) or autoionization (e.g., high-lying Rydberg states) upon collision with the CEM. Ions and excited neutrals were distinguished by comparing intensity measurements made with positive and negative biases on the

[a] Permanent address: Department of Physics, Wesleyan University, Middletown, CT 06457-6036.
[b] Permanent address: Chemistry Division, Naval Weapons Center, China Lake, CA 93555-6001

 0021-8979/90/083641-11$03.00

CEM front cone. The CEM front cone was typically masked so that only a small portion was in line-of-sight with the sample to prevent detector saturation.

A Bessel box energy analyzer, described by Craig and Hock,[10] could be placed between the sample and the CEM to provide low-resolution energy analysis of the charged particles.

Mass determination of the ground-state neutral particles was obtained with a Finnegan Model 4001 quadrupole mass spectrometer (QMS) with a CEM detector. With the ionizer "on" and the axis of the QMS aligned to provide a line-of-sight path from the target through the QMS to the CEM, both excited neutrals and ionized ground state neutral particles were detected. Positive-ion-mass determination was obtained with a UTI Model 100C QMS with the ionizer removed. The potential on the focus plate in front of the mass filter was varied to maximize collection and focusing of the externally generated ions. Line-of-sight was avoided to prevent detection of excited neutrals. Calibration of the quadrupoles was checked by leaking in Kr providing singly ionized peaks at 80, 82, 83, 84, and 86 amu as well as well resolved doubly ionized peaks at 42 and 43 amu.

Measurements of light emission from excited species in the near-surface region were made initially with a Gencom Thorn EMI Model 9924QB photomultiplier tube (PMT) with a quartz window, positioned at the end of a silica fiber optics cable mounted on a vacuum system flange. The target end of the fiber optics cable was equipped with a slit aperture and collimating lenses to ensure that only light directed along the axis of the cable (perpendicular to the target surface normal) was detected. This allowed localizing the region of space probed by the detector, e.g., for the observation of temporal variations in light intensity as light emitting atoms/molecules passed in front of the slit. For spectral analysis of this spatially selected light, the output of the fiber optic cable was attached to a Thermo Jarrell Ash Monospec-18 spectrometer employing a 150-lines/mm grating. An EG&G Model 1421 gated, intensified, position-sensitive detector responsive to light in the region between 200–830 nm was used with an EG&G Model 1460 optical multichannel analyzer to acquire both time-averaged and time-resolved spectra.

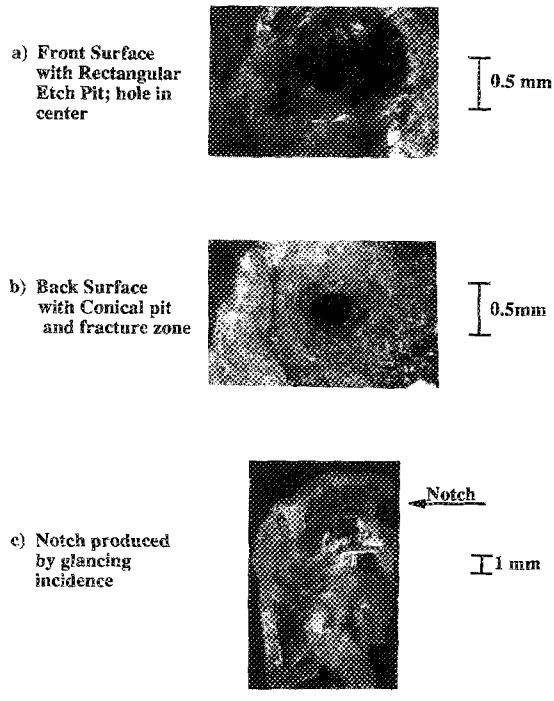

FIG. 1. Optical microscope images of the front and back surfaces of an RDX crystal after bombardment with a 248-nm excimer laser light. The front surface (a) shows the etch pit with a circular hole passing through the entire crystal. The back surface (b) shows the hole opening into a conical structure lined with extensively fractured material. (c) The consequences of glancing incidence on the side of the crystal: A clean notch is etched.

III. RESULTS

A. Surface topography

When crystals of RDX are exposed to 248-nm excimer laser light at fluences $\geqslant 90\ \mathrm{mJ/cm^2}$, we observe etching of the crystal in the shape of the laser beam. No "pre-exposure" of repeated laser pulses was required before etching commenced. No evidence of any residue or surface melting was observed. Etch rates were not measured but showed a very strong fluence dependence, increasing rapidly with increasing fluence. On crystals that displayed different facets there was no apparent dependence of the etch rate on surface crystal orientation. At fluences $\geqslant 150\ \mathrm{mJ/cm^2}$ the crystal usually exhibited extensive internal fracture and frequently shattered into small pieces.

Thinner crystals (< 1 mm) showed ablation from the back side in addition to the front side. Whereas the etch pit on the front side was rectangular (shape of the laser profile), the back pit was circular in cross section. One sample formed a clean 50-μm hole at the center and bottom of the front surface rectangular pit [see Fig. 1(a)] which opened into a rough, conical etch pit on the back side [Fig. 1(b)]. The roughness on the back side was due to multiple fracture, whereas the hole was cleanly etched with no appearance of melting or fracture. A slightly thicker sample also showed ablation from both front and back with no hole formed in the front etch pit, suggesting that the hole is eaten from the *backside* towards the front. The hole shows circular symmetry about the center of the rectangular laser beam. This indicates that decomposition is nucleating at the most intense part of the laser spot in a rather nonlinear fashion. Close examination of the walls of the hole showed some crystallographic-like facets.

At fluences of $1\ \mathrm{J/cm^2}$ we calculate a radiation pressure pulse of $< 10^4\ \mathrm{N/m^2}$ which is too small to cause the extensive fracture we observe. More likely, pressure arises from conversion of solid RDX to gaseous products, similar to the effects described by McBride,[11] and the change in volume results in fracture. When the back of the crystal is ablating, at higher fluences one could observe small fragments being ejected from the crystal.

Figure 1(c) shows the effect of a glancing incident laser on the edge of the crystal, namely producing a clean notch. Other parts of this crystal were also hit by the laser at earlier times.

TABLE I. QMS detected mass peaks due to neutral emission from laser bombardment of RDX.

Approximate threshold (mJ/cm^2)	Mass (amu)	Assigned parent(s)	Relative intensity at 125 mJ/cm^2
5	46	NO_2	6
5	30	NO, H_2CO	100
5	28	N_2, H_2CO, CO	86
5	27	HCN	97
5	26	CN, HCN	57
5–10			
5–10	44	N_2O	21
5–10	42	C_2H_4N and/or CH_2NN	8
5–10	29	H_2CO	22
5–10	18	H_2O	93
5–10	17	OH, H_2O	85
5–10	16	O, NO, H_2O	39
5–10	15	NH, $NO^{(2+)}$, C_2H_4N, and/or CH_2NN	27
5–10	14	N, CN, HCN, NO, N_2O	63
5–10	13	CH, H_2CO, C_2H_4N, and/or CH_2NN	20
5–10	12	C, CN, HCN, CO	52
20	2	H_2; higher mass parents	39
The following extremely small peaks were detected at 125 mJ/cm^2 only under conditions of reduced laser spot size; the intensities are given relative to mass 30 acquired at the same reduced spot size.			
	120	$CH_2NNO_2NO_2$	0.5
	81–83	$C_3N_3H_x + H_x$ $(x = 0,1,2)$	~1
	75	$CH_2NNO_2 + H$	5
	52,54,56	$CH_2CH_2N_2 - H_x$ $(x = 0,1,2)$	2.5

B. Ground-state neutrals

Copious neutral gas emission from the crystal was observed. At high laser fluences, a nearby Bayart-Alpert pressure gauge would show an order of magnitude increase in vacuum system pressure (10^{-5} to 10^{-4} Pa) with each laser pulse. With the Granville-Phillips QMS (ionizer on) we measured the mass of the emitted neutral species. At low fluences (~5 mJ/cm^2) the ion mass peaks generated from ionization of neutral species consisted of only five masses (46, 30, 28, 27, and 26). By analysis of expected cracking fractions and time distributions, these appear to be small mass dissociative products with no additional fragmentation and can be assigned to the parent species shown in Table I. As the fluence is increased to ~5–15 mJ/cm^2, additional peaks appear, again assigned by taking into account cracking fractions and time distributions, shown in Table I. At fluences $\geqslant$20 mJ/cm^2, mass 2 appears and grows with increasing fluence and is assigned to both H_2 and higher mass parents containing hydrogen.

In Fig. 2, we plot the detected signals (versus time) for the QMS set at the masses shown and a fluence of 125 mJ/cm^2. Intensity units for these plots are arbitrary, but relative intensities at this fluence are given in Table I in the right-hand column and shown plotted in Fig. 3. Due to interference with the ion blast, our quadrupole mass spectrometer could not resolve mass 1 so that we were not able to determine conclusively if atomic hydrogen was a product. The higher mass peaks (> 52 amu) were found only after extensive searching and reduction (by masking) of the spot size of the laser beam hitting the sample. As we shall discuss below, both the fluence and the spot size greatly affected the physical and chemical processes triggered by the laser. Unless stated otherwise, the laser beam was unmasked and therefore full size (0.5×1 mm^2).

If one takes the product distribution for the unmasked bombardment and assumes standard cracking fractions for the "parent" products (at 70-eV electron bombardment energy), one calculates C:N:O:H ratios of approximately 1:2:2:2, which is in agreement with the stoichiometry of the RDX molecule. The intense peaks are fragments $\leqslant$mass 46 which suggests that the decomposition paths are nearly complete. All of the molecular species $\leqslant$mass 46 observed here are seen in both ir multiphoton dissociation[5] and thermal decomposition[12–14] of RDX. The atomic emission and the extremely small contributions above mass 46 differ dramatically from these other forms of decomposition. We searched carefully under a variety of laser beam conditions for mass 74 (the concerted decomposition product seen in Ref. 5) but never observed it—a small mass 75 was observed, as mentioned above and attributed to $CH_2N_2O_2 + H$. However, we note that the ratio of H_2CO/N_2O is seen to be near unity, consistent with one of the decomposition paths of the concerted decomposition intermediate $CH_2N_2O_2$ namely,

$$CH_2N_2O_2 \rightarrow H_2CO + N_2O. \quad (1)$$

We also note that the ratio of HCN/H_2CO is roughly 5, which is consistent with HCN being created by the second decomposition path,

$$CH_2N_2O_2 \rightarrow HCN + HONO \quad (2)$$

at very close to the same branching ratio reported by Zhao and co-workers.[5]

Although the reaction pathways are not completely defined by our data, our results suggest decomposition consistent with the computer fits to the major TOF peaks shown in Fig. 2. The individual curves show the fraction of each parent mass which is assumed to be created at or near the time of the laser pulse and which travels to the ionizer as the parent. The TOF model curves were generated from Maxwellian velocity distributions corresponding to two temperatures, namely 1100 and 3000 K. Obviously, if the laser fluence is changed, the observed shifts in the TOF curves would require changes in this temperature, namely increasing fluence would result in higher equivalent temperatures. The use of two temperatures is only for convenience; temperature versus time distributions would be more appropriate. Nevertheless, the fits in general are fairly good, requiring a relatively small number of parent molecules in comparison with multiphoton ir dissociation.[5] Note that some of the products required only one temperature, namely ~ 1100 K for CN(26), H_2CO(29), and masses 40–46 amu. The TOF curves seen for the very small peaks at masses 52, 54, 56 showed broad structures perhaps due to dissociation of heavier components.

Although HONO is a likely product in our study, it was not directly detected as mass 47, nor were significant amounts of mass 47 required to fit our mass 30, 17, and 16 TOF peaks (the cracking pattern of HONO produced by electron bombardment[5] contains little, if any, mass 47). Oyumi and Brill[14] have pointed out that in studies of RDX thermal decomposition, heterogeneous (in our case surface-gas-phase components) and gas phase reactions can lead to C-N bond cleavages, producing N_2O, H_2CO, whereas N-NO_2 bond cleavage is most likely in the condensed phase yielding HCN without producing equivalent amounts of HONO. They also showed that at heating rates of ~ 50 K/s and pressures of 1 and 70 atm there was a significant shift in products with increasing pressure due to reactions involving gas phase collisions versus direct thermolysis reactions. Thus, our lack of direct detection of HONO may be due to similar collisional effects.

C. Excited neutrals

At fluences $\geqslant 100$ mJ/cm^2, a fast signal appears that has the following properties:

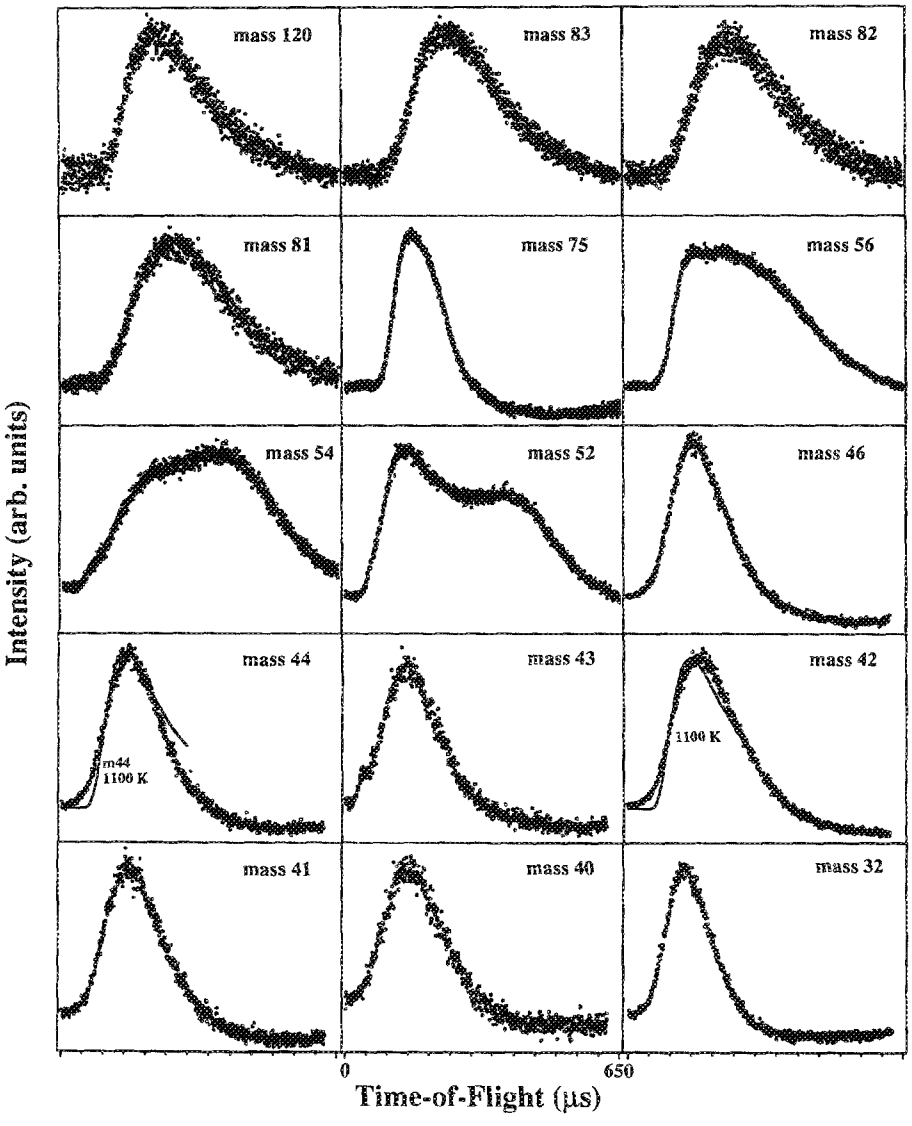

FIG. 2. The detected time-of-flight curves for the observed neutral species emitted from the front surface of the RDX crystal acquired with a quadrupole mass spectrometer. The laser fluence was 125 mJ/cm^2. The curve fits shown for the major peaks are superpositions of Maxwellians for the parent masses and effective temperatures shown.

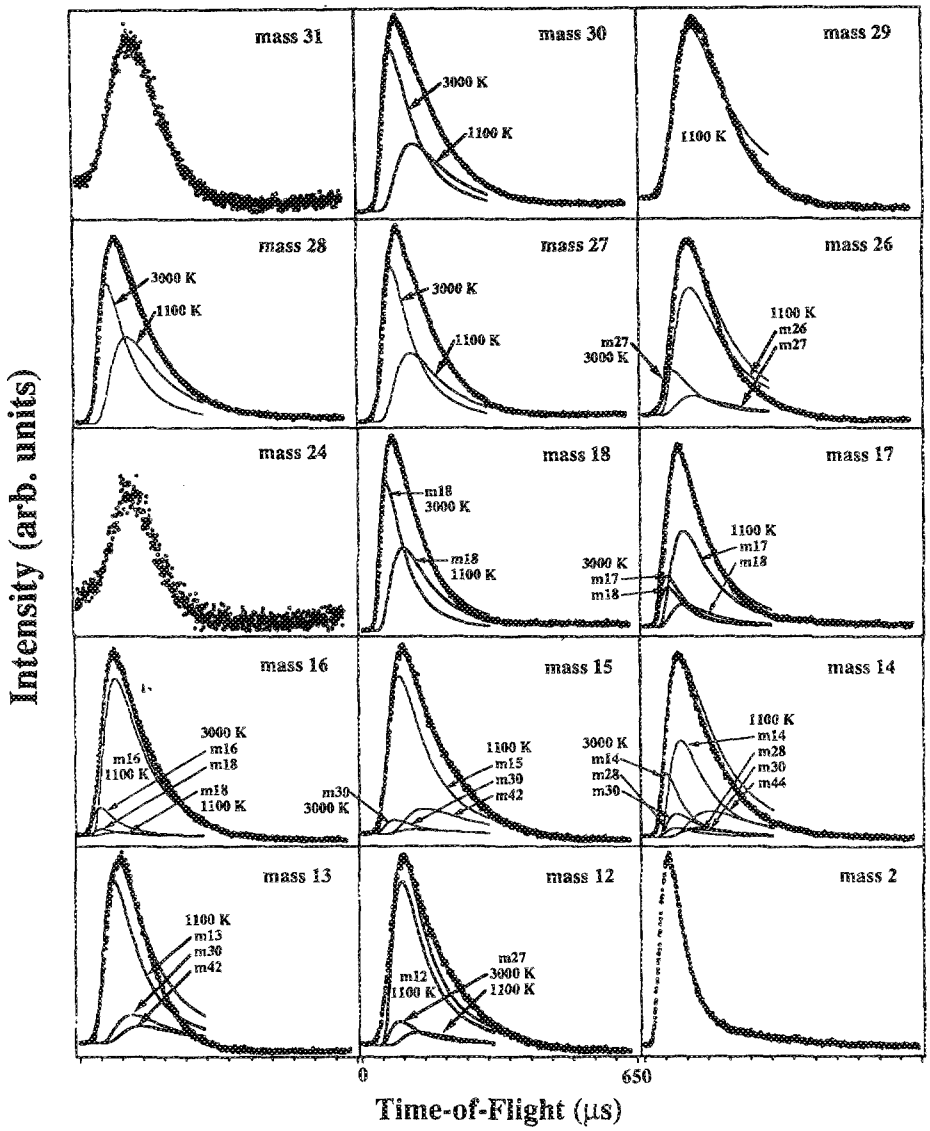

FIG. 2. (*continued*).

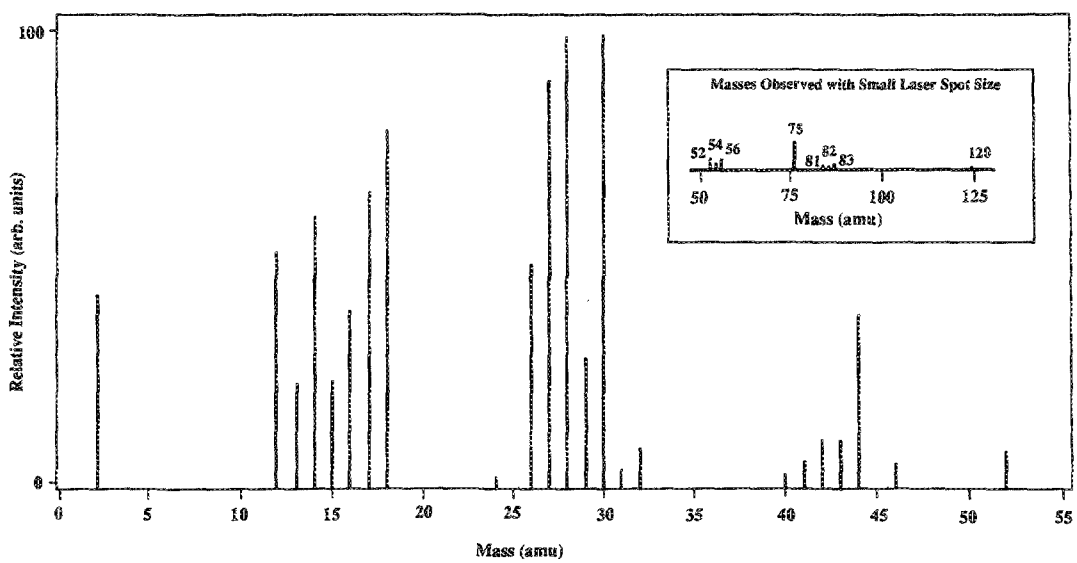

FIG. 3. The relative intensities of the quadrupole mass spectrometer signals for data shown in Fig. 2. The inset shows the intensities for the peaks observed with reduced laser spot size.

(1) The signal is very sensitive to alignment of the irradiated point on the sample and the QMS—strict line-of-sight is required from the surface to the CEM. If a silica window was placed in front of the entrance to the ionizer, no signal was observed (therefore, energetic photons due to collisions with surfaces could be ruled out).

(2) The signal is detected by the CEM with unshifted peak position independent of the following conditions: (i) ionizer on/ionizer off; (ii) mass filter on/mass filter off; (iii) mass setting, with mass filter on; and (iv) the presence of $\pm$ voltages on all ionizer electrodes (positioned at the entrance to the mass filter). We have reported on similar long lifetime, excited neutral signals originating from laser bombardment of polymers[15] and a sodium trisilicate glass.[16] We provided evidence that such signals were due to neutral atoms/molecules in an excited electronic state (e.g., a metastable or long-lived Rydberg level). We have argued that the production of such fast species occurs via reneutralization of *ionic* species leaving the material. Simple, nondissociative ion-electron recombination in the gas phase requires a third body to conserve energy and momentum; thus, collisions with other gaseous species is a strong requirement. As mentioned earlier, in all of these materials, including RDX, there are high densities of gas created with each laser pulse which can provide a third body.

A series of excited neutral time distributions is shown in Fig. 4 for a number of laser fluences. Note that the TOF peak position decreases only slightly with increasing fluence, whereas the intensity increases dramatically with fluence, changing by a factor of more than 350 for an increase of a factor of 10 in fluence (from 70 to 700 mJ/cm^2). The detection of such a particle is likely by collisional de-excitation at the front surface of the CEM ($\sim$5 eV). Obviously, the lifetime of these particles must be $\sim$50 μs or longer. Well known long-lived metastable and Rydberg states occur in H_2, N_2, NO, and CO, and CO_2.[17,18] We present evidence

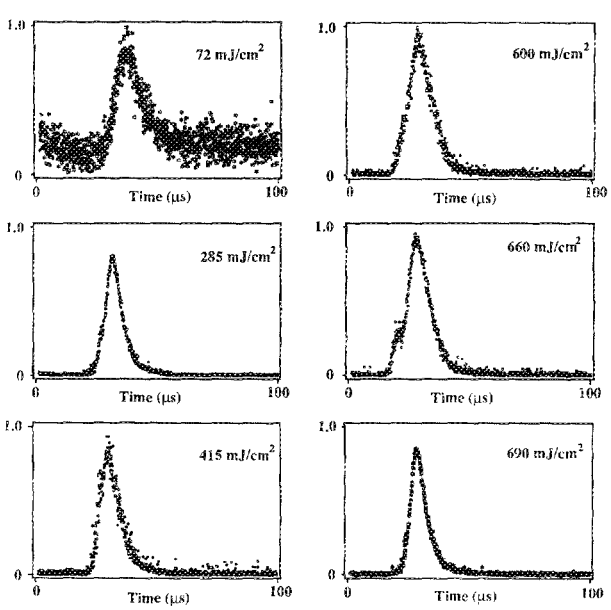

FIG. 4. The excited neutral time-of-flight distributions acquired at different laser fluences.

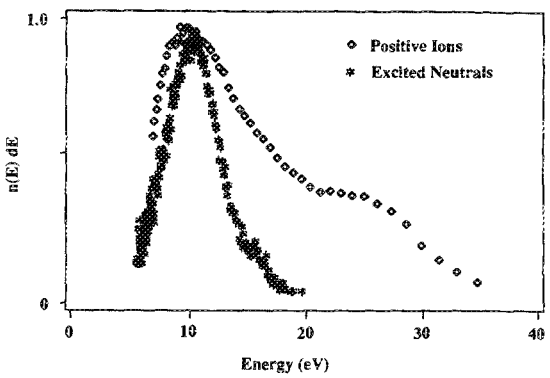

FIG. 5. Energy distribution curves for the excited neutral (with an assigned mass of 30 amu) and the mass 30 ion signal, assigned to NO^+. The strong similarity in these energy distributions supports the mass 30 assignment for the excited neutral.

below that the mass of this excited species is 30 amu and is therefore very likely NO*. Accepting this mass, the kinetic-energy distribution of this excited particle is shown in Fig. 5 for a laser fluence of 300 mJ/cm^2, showing a maximum at $\sim$10 eV and extends out to over 15 eV. Such kinetic energies are clearly nonthermal *and* are also too high to arise from a simple photodissociative process.

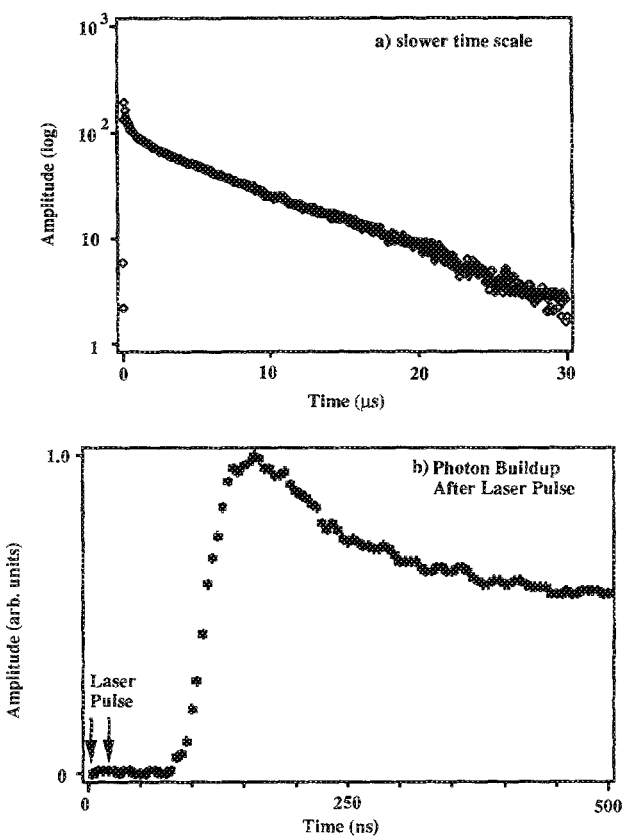

FIG. 6. (a) Photon emission from the surface region of the crystal showing the time dependence of the near UV-VIS emission relative to the laser pulse; (b) the time interval near the time of the laser pulse.

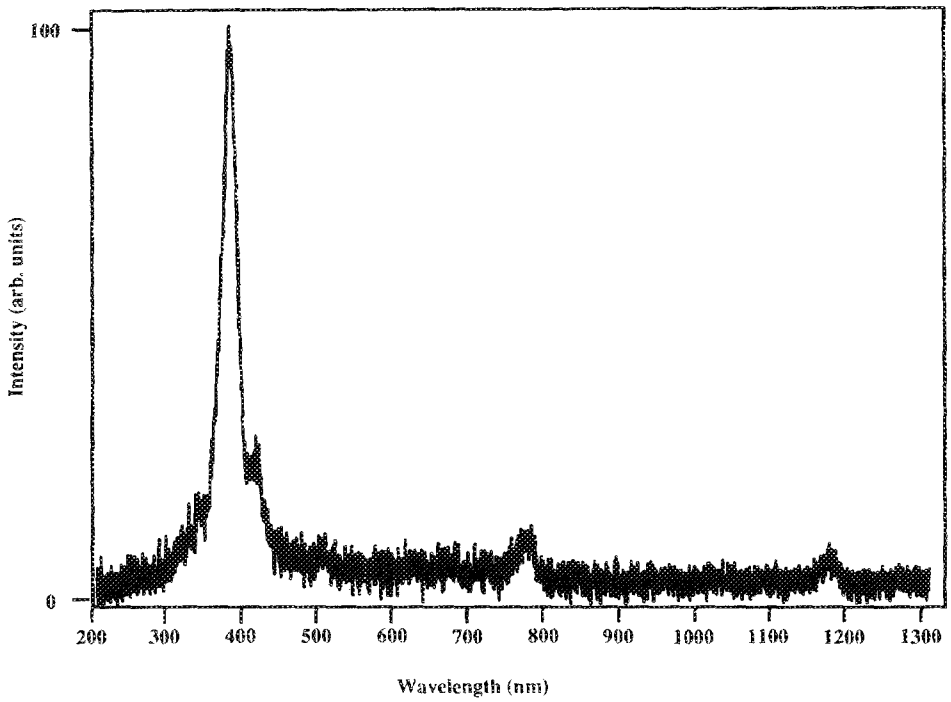

FIG. 7. The spectrum of the photon emission emitted from near the sample surface over the time interval 200 ns to 1.2 μs after the laser pulse.

D. Photon emission

We continued the search for other evidence of products in excited states by examining the near-surface region of the RDX crystal for visible light emission. Other than fluorescence in the crystal itself, the only light detected occurred directly at the surface of the crystal. Figure 6(a) shows the *total* near UV-visible emission (log intensity scale) versus time on a relatively slow time scale, for a laser fluence of 130 mJ/cm^2, measured with a fiber optics bundle pointed directly at the crystal surface coupled to a photomultiplier (PMT). Figure 6(b) shows on a linear intensity scale and faster time scale, the rise in photon intensity versus time, where $t = 0$ represents the beginning of the laser pulse. We note from these two curves that there is a clear *delay* in the build up of the light emission after the laser pulse and the light is sustained for several tens of microseconds. Using the time resolution capabilities of the optical multichannel analyzer, we analyzed the emission spectrum versus time after the laser pulse. Figure 7 shows the resulting low-resolution emission spectrum taken at a fluence of 600 mJ/cm^2, acquired over a 1-μs time interval, starting 200 ns after the onset of the 20-ns laser pulse. The spectrum remains unchanged over the time interval of a few μs after the laser pulse where it is eventually lost in noise. The spectrum is due entirely to the allowed $B\,^2\Sigma^+ \rightarrow X\,^2\Sigma^+$ transitions in the diatomic radical CN (the features at $\sim$775 and 1160 nm are higher-order diffraction peaks). There is no evidence of the RDX fluorescence and phosphorescence spectra seen by Marinkas.[19] The RDX fluorescence *should* be missing due to the 100-ns delay—Marinkas reports a lifetime < 2 ns. If we probe the light emission with either the PMT or the spectrometer just a few cm further out from the surface (i.e., *not* viewing the surface) no detectable light is observed. Since the lifetime of the CN $B\,^2\Sigma^+$ states are $\sim$60 ns,[20] any CN* created at the surface could only travel distances < 0.1 cm from the surface and therefore these states are being *created* at times considerably longer than the duration of the laser pulse. Two important conclusions are suggested.

First, the production of CN* is occurring after laser stimulation on a time scale of $\sim$100 ns in a expanding reaction zone due to pressure dependent chemistry. A likely mechanism for this creation on such a long time scale is chemiluminescence involving products from the decomposition. For example, CN $B\,^2\Sigma^+ \rightarrow X\,^2\Sigma^+$ chemiluminescence has been shown to arise from the following reactions (from Refs. 21, 22, and 23, respectively):

$$C + NO \rightarrow CN^* + O,$$

$$C^+ + N_2O \rightarrow CN^* + NO^+,$$

$$C_2(a^3\Pi) + NO \rightarrow CN^* + CO.$$

Similarly, Faust *et al.*[24] have suggested that delayed, pressure-dependent chemiluminescence they observed following photofragmentation of a variety of simple molecules was due to ion-molecule reactions following stimulation.

Second, to produce a 10–100 μs duration in the creation of CN*, the reactants must be produced for times of several tens of microseconds after the laser pulse. We therefore conclude that there is a sustained exothermic reaction at the RDX surface, originally ignited by the laser, continuing *after* the laser pulse. For the fluences used here, this reaction builds up in a few tens of ns, then dissipates on the time frame of 10–10^{12} μs as opposed to running away due to some form of dissipation (e.g., thermal conductivity) which counters the growth of the energy releasing decomposition.

E. Sustained emission of neutral species

To prove that such sustained reactions are present, we constructed a "total neutral-emission" probe, drawn schematically in Fig. 8(a), consisting of an ionizer from a QMS

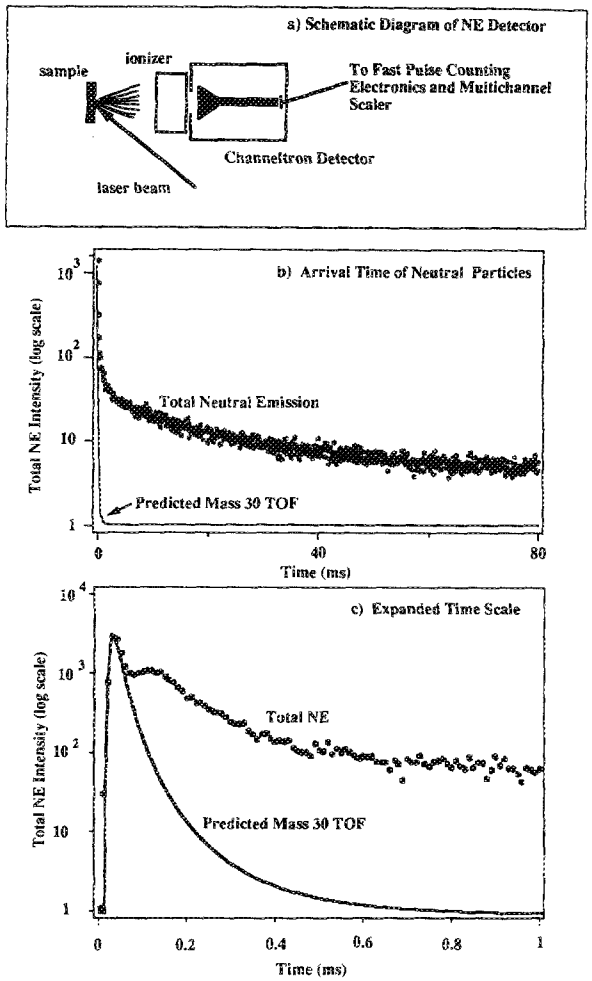

FIG. 8. (a) Schematic diagram of the neutral emission detector for probing in a very sensitive way the total gaseous emission following the laser pulse. (b) The resulting pulse-counted emission for a time period of 80 ms. The solid curve shows the mass 30 emission which would be detected at the position of the ionizer used in this study (4 cm). (c) The first 1 ms of the above data.

followed directly by an electron multiplier (CEM) placed out of direct line of sight. To increase our sensitivity to low fluxes of neutrals, we ran the CEM in a pulse-counting mode (thus, every ion detected by the CEM was converted to a countable pulse). Without any incident laser light, the background gases led to negligible counts during data acquisition. The resulting signal (ion counts/1 μs time interval) from incident neutrals accumulated for 20 successive laser pulses ($t = 0$) is shown in Fig. 8(b) and on an expanded time scale, Fig. 8(c). If we generate the appropriate time-of-flight distribution for the heaviest of the major neutral species, mass 30, by transforming the mass 30 curve fit for the data shown in Fig. 2 to appropriate shorter times due to a shorter flight path, we see the superimposed curves shown with solid lines, again plotted on a log scale to emphasize trends at long times. Under this high-sensitivity pulse counting mode of acquiring neutral emission, we see that the tail is, in fact, sustained well after the decay of the faster component and is consistent with the above interpretation of a sustained decomposition reaction. For the initial steep part of the decay, the time constant is nearly equal to the decay in the photon emission (attributed to excited CN*) observed after the laser pulse. Thus, these signals serve as evidence that at the completion of the laser pulse, there is a continuation of the decomposition which damps out in a few milliseconds. This long decay cannot be attributed to pump out of our vacuum system in response to a pressure pulse; the latter has a measured characteristic decay constant of ~400 ms which probably corresponds to the flat part of these curves.

One further attribute of the mass selected neutral emission not discussed above, which suggests that a reaction is being induced in the crystal, is that we discovered that at constant fluence (incident laser energy per unit area) masses above mass 46 were detectable only if we reduced the spot size of the bombarded region. Figure 9 shows the intensity of (a) the mass 75 peak and (b) the total pressure increase as a function of spot size, both of which are clearly nonlinear. As the spot size is increased, mass 75 first rapidly increases, then decreases to zero; the other masses above 50 amu behave similarly. The total pressure change (representing the total amount of gas released per laser shot) increases nearly exponentially with spot size (the detector used for this measurement saturated at ~0.3-mm^2 spot size—thus terminating the curve).

If the neutral emission were caused by a mechanism that

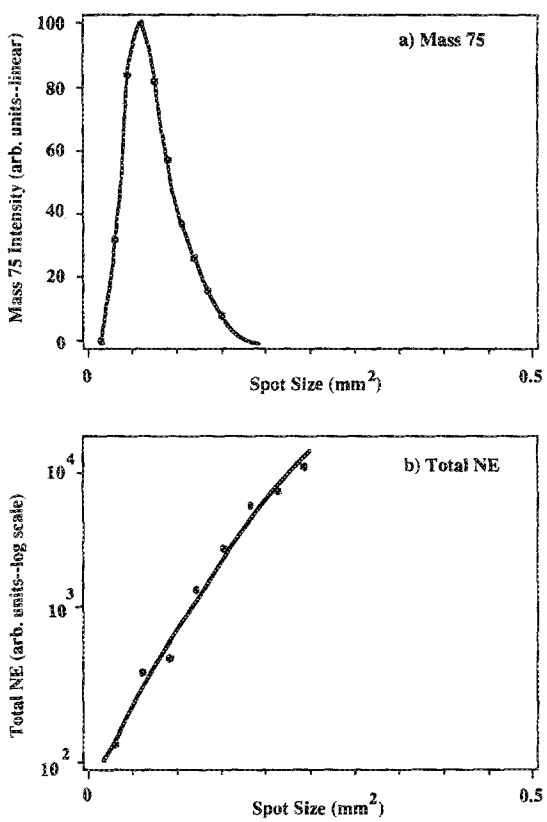

FIG. 9. (a) The emission intensity (arbitrary units—linear scale) for mass 75 vs spot size of the focused laser beam on the crystal surface. The laser fluence was kept constant at 120 mJ/cm^2. (b) The total pressure change (arbitrary units, log scale) from ablation of the RDX at the same laser fluence (120 mJ/cm^2) vs spot size.

only involved the number of photons striking each absorption center, there should be a simple linear dependence of the individual products and total gas emission on the spot size. On the contrary, this area (volume) effect suggests that the effectiveness or probability of igniting a sustained decomposition reaction increases and this reaction propagates into a larger portion of the crystal in a nonlinear fashion as more of the crystal is exposed to the laser. The disappearance of masses 52–120 amu at larger spot sizes is perhaps caused by higher numbers of collisions of these heavier products with other gas molecules due to a significant increase in gas density, which result in their demise.

F. Positive- and negative-ion emission

Preliminary studies of the charged-particle emission from RDX show the emission of positive ions over a wide range of fluences. In near-field free-drift conditions, the positive ions exhibit velocities of similar magnitude to the excited neutral emission, showing an increase in velocity with fluence. By slight displacement of the QMS from direct line of sight to the bombarded region we were able to separate the excited neutrals from the positive-ion emission (PIE) and achieve mass selection and therefore determine the ion masses. Figure 10 shows the signals corresponding to the only three positive ion species detectable above our noise, namely, 30, 18, and 42 amu, acquired at a fluence of 350 mJ/cm^2. Their relative intensities are approximately 100:8:3, respectively, and we assign to these masses NO, H_2O, and CH_2NN and/or C_2H_4N. Although these correspond to large peaks with the same identity in the LIMA measurements of Tang *et al.*, they see larger peaks which are completely missing from our PIE spectrum (e.g., 12 [C^+], 15 [CH_3^+], and 27 [HCN^+]—Tang's assignments shown in square brackets).

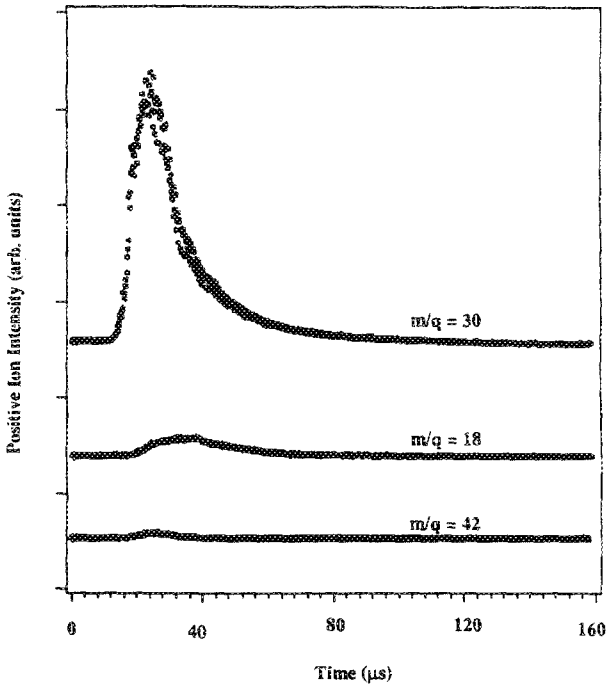

FIG. 10. Positive-ion signals corresponding to quadrupole mass filter settings of 30, 18, and 42 amu. Laser fluence = 350 mJ/cm^2.

In our case, most of the emitted ions are mass 30 (NO^+). Letting *all* of the ions drift under essentially field-free conditions (there is some field penetration of the front cone of the CEM detector tending to accelerate ions near the completion of their flight path), the resulting TOF can be transformed into an energy distribution which we attribute to the dominant mass 30 ions. The resulting distribution function is shown in Fig. 5 (symbol: ◇) for a laser fluence of 350 mJ/cm^2, approximately the fluence used to generate the excited neutral-energy distribution (symbol: *). The ion-energy distribution (◇) is consistent with initial kinetic energies calculated from the mass selected mass 30 ion data (e.g., Fig. 10) where the flight path purposefully included applied accelerating fields. From Fig. 5, we see that the PIE energy distribution peaks at ~10 eV, and is quite similar to the excited neutral-energy distribution if we allow for some broadening of the ion distribution due at least partially to stray E fields. The similarities in these energy distributions provides strong evidence that the excited neutral is a mass 30 ion which has been (a) accelerated away from the surface, and (b) neutralized in the near-surface region where collisions can occur with high frequency. This mass 30 PIE time-of-flight signal is considerably faster than the slower ground-state neutrals, e.g., as shown in Fig. 2, which we have attributed primarily to NO. The NO molecule is known to have one long-lived excited state, namely the $a^4\Pi$ state, with a lifetime >0.1 s and lying 4.8 eV above the ($X^2\Pi$) ground state.[25] A second state with possible long lifetime is the $b^4\Sigma^+$ which lies 6 eV above the ground state. In terms of detection by impact with the CEM front cone surface, the latter is more likely to release electrons by deexcitation. We therefore attribute the formation of this excited species to the collisional reneutralization of energetic NO^+ into a long-lived excited state of NO.

There appears to be little evidence of laser-plume interactions such as seen in excimer laser irradiation of polymers and glass reported earlier. The latter could cause acceleration of positive ions as explained in Ref. 15. In RDX a more likely source of PIE kinetic energy is an electrostatic effect. The rapid removal of photoelectrons from the crystal leaves behind a distribution of positive charge which can accelerate the positive ions away from the surface. The resulting ion energy distributions are thus a measure of the electrostatic potentials at the positions where the ions were created. A simple electrometer measurement with an electrode placed on the edge of one of the RDX crystals confirmed that the crystal was charging positively upon incidence of laser light. In addition, copious electron emission was detected using a Channeltron biased positively. The electron emission was confirmed by the submicrosecond time-of-flight of negative charge at a detector several cm away from the bombarded region.

For the sake of completeness, the emission of negative ions were also observed, as indicated by microsecond flight times. These negative ions exhibited TOF behavior consistent with ionic species over a range of masses somewhat low-

er than the positive ions, although we have not as yet determined their masses nor kinetic energies. Tang *et al.*[4] observed intense negative-ion emission from RDX (at 266 nm) corresponding to CN^-, $CH_2N_2^-$, and perhaps $CNCH_2NO^-$ in addition to other masses.

IV. DISCUSSION

Neither a simple photochemical nor photothermal mechanism can explain all of these observations. The following preliminary model is proposed for the ablation process observed in RDX.

(1) Under laser irradiation, photochemical and possibly photothermal decomposition of the RDX molecules is initiated in the surface and near-surface region of the crystal. As a function of fluence, the penetration of higher-intensity UV into the crystal and therefore the depth of the process zone increases. Electrons and ionic products are produced by photonic processes (nonthermal). Some heating of the surface due to laser absorption does occur, however, via vibronic transitions. The exothermicity of the decomposition results in 0–1-eV kinetic energies of fragments in regions of high density. Thus, chemical energy, converted to kinetic energy of the fragments leads to thermalization in the near-surface region. Consequently, many of the uncharged products have a Maxwellian velocity distribution, consistent with the establishment of equilibrium. We propose that the higher temperature (i.e., 3000 K) portions of the time-of-flight curves seen for example at 18, 27, and 30 amu correspond to the laser-induced decomposition.

(2) The initial excitation liberates sufficient energy to initiate a self-sustaining decomposition reaction which appears to reach a peak in ~ 100 ns and lasts for tens of microseconds after the laser pulse. The effective temperature of this chemistry is lower (~ 1100 K); masses 26 and 29 were dominated by this low temperature component in the time-of-flight curves.

(3) The removal of the NO_2 from the RDX molecule may occur in a direct fashion without an intermediate. Several other products are consistent with secondary decomposition paths from the concerted decomposition intermediate $CH_2N_2O_2$ discussed by Zhao and co-workers.[5]

(4) The 383-nm photon emission seen at the surface over several microseconds in duration is attributed to chemiluminescence from CN. This is consistent with the continuation of the decomposition reaction some time after the laser pulse, which serves as a source of reactants to create the CN*.

(5) At constant laser fluence (energy/area) the onset of the sustained decomposition reaction depends on the size of the laser beam due to a volume effect regarding the transport of energy between portions of the crystal. The highly localized holes observed in some of the crystals are attributed to the etching occurring during the sustained reaction. When extensive decomposition occurs inside the crystal (e.g., at high fluences), sufficient pressures build up to result in fracture. When such fracture occurs on the back side of the crystal, gases blowing off the backside carry away ejecta (micron-sized pieces) produced by fracture. Increasing the size of the irradiated spot (at constant fluence) changes dramatically the extent of the decomposition reaction and can affect the products observed away from the surface. Larger spot size may result in a more intense sustained reaction through collective processes and and/or limited transport of heat away from the reaction zone.

(6) Recombination chemical reactions are occurring: Products such as H_2O, N_2, and NH are likely due to collisional reactions occurring in the process zone.

(7) Evidence for the occurrence of dynamic gas-phase processes are seen in the existence of the excited neutral species as well as the high-metastable and ion-energy distributions. The similarities between the excited neutral and the 30-amu positive ion leads us to propose that the excited neutral is NO in a long-lived electronic excited state created by reneutralization of energetic NO^+ ions. The combination of high kinetic energy and charge (or in the case of the excited neutral, several eV of internal electronic energy) takes a large amount of energy per particle away from the reaction zone.

(8) Negative ions may be a result of photoelectron collisions (at low energies) with molecular species in the process of dissociating (or remnants from earlier laser pulses).

V. CONCLUSIONS

Bombarding RDX with 248-nm laser pulses at fluences of 5–750 mJ/cm^2 results in a wide range of effects including photoelectron emission, production of $\pm$ ions, ground-state neutrals (2–120 amu), excited neutral CN, a long-lived excited neutral species identified as NO*, ablative etching of the crystal, and at higher fluences fracture of the crystal. We have presented evidence for the ignition of a sustained decomposition reaction which continues many tens of μs after bombardment. A number of additional studies are suggested such as the following:

(i) Developing a more detailed model for the production of the principle neutral species and explaining their velocity distributions.

(ii) Addressing a number of issues regarding the "hot" component in the neutral emission vs "cooler" component, i.e., proving that the former is directly laser induced and the latter is coming from the self-sustained reaction that follows. The corresponding reaction paths for these two types of emission are needed. Comparing measurements of front-side/backside emissions might be one way to proceed.

(iii) Carrying out a more detailed examination of the reactions creating the CN* and NO*.

(iv) Examining in more detail the etching of holes and phenomena responsible for fracture by laser bombardment.

(v) Probing the laser wavelength dependence of these phenomena.

(vi) Probing the spatial distributions of the gaseous products, similar to Parr's studies[26] of combustion of RDX using planar laser-induced fluorescence imaging.

ACKNOWLEDGMENTS

This work was supported by the Office of Naval Research Contract No. N00014-87-K-0514, Dr. R. S. Miller, Program Manager, and the Washington Technology Center.

We wish to thank Mark Dexter for his assistance in carrying out these experiments.

[1]R. Srinivasan, Science **234**, 559 (1986).
[2]W. A. Schroeder, P. E. Wilcox, K. N. Trueblood, and A. O. Dekker, Anal. Chem. **23**, 1740 (1951).
[3]L. C. Yang and V. J. Menichelli, Appl. Phys. Lett. **19**, 473 (1971).
[4]T. B. Tang, M. M. Chaudhri, C. S. Rees, and S. J. Mullock, J. Mater. Sci. **22**, 1037 (1987).
[5]X. Zhao, E. Hintsa, and Y. T. Lee, J. Chem. Phys. **88**, 801 (1988).
[6]R. Engelke, W. L. Earl, and C. McMichael Rohlfing, J. Phys. Chem. **90**, 545 (1986).
[7]J. T. Hagan and M. M. Chaudhri, J. Mater. Res. **12**, 1055 (1977).
[8]P. J. Halfpenny, K. J. Roberts, and J. N. Sherwood, J. Mater. Sci. **19**, 1629 (1984).
[9]C. S. Choi and H. P. Boutin, Acta Crystallogr. Sect. B. Struct. Crystallogr. Cryst. Chem. **26**, 1235 (1970).
[10]J. H. Craig and J. L. Hock, J. Vac. Sci. Technol. **17**, 1362 (1980).
[11]J. M. McBride, B. E. Segmuller, M. D. Hollingsworth, D. E. Mills, and B. A. Weber, Science **234**, 830 (1986).
[12]M. Faber and R. D. Srivastava, Chem. Phys. Lett. **64**, 307 (1979).
[13]R. Behrens, Jr., in Proceedings of NATO Advanced Studies Institute on Chemistry and Physics of Energetic Materials, September, 1989, Altavilla, Milicia, Sicily, edited by S. Bulusu (unpublished).
[14]Y. Oyumi and T. B. Brill, Combust. Flame **62**, 213 (1985).
[15]K. Tonyali, L. C. Jensen, and J. T. Dickinson, J. Vac. Sci. Technol. A **6**, 941 (1988).
[16]P. A. Eschbach, J. T. Dickinson, S. C. Langford, and L. R. Pederson, J. Vac. Sci. Technol. A (to be published).
[17]E. E. Muschlitz, Jr., in *Molecular Beams*, edited by J. Ross (Wiley Interscience, New York, 1966).
[18]R. S. Freund, in *Rydberg States of Atoms and Molecules*, edited by R. F. Stebbings and F. B. Dunning (Cambridge University Press, Cambridge, 1983), pp. 355–392.
[19]P. L. Marinkas, J. Lumin. **15**, 57 (1977).
[20]H. Okabe, *Photochemistry of Small Molecules* (Wiley Interscience, New York, 1978), p. 198.
[21]D. Brandt and Ch. Ottinger, Chem. Phys. Lett. **23**, 257 (1973).
[22]M. Tsuji, I. Nagano, T. Susuki, K. Mizukami, H. Obase, and Y. Nishimura, J. Phys. Chem. **90**, 3998 (1986).
[23]J. B. Lurie and M. A.El-Sayed, J. Phys. Chem. **84**, 3348 (1980).
[24]W. L. Faust, B. B. Craig, S. Chattopadhyay, and R. G. Weiss, J. Phys. Chem. **91**, 54 (1987).
[25]E. Miescher and K. P. Huber, in *Physical Chemistry: Series Two, Volume 3, International Review of Science*, edited by A. Buckingham (Butterworths, London, 1976), pp. 37–74.
[26]T. Parr, Naval Weapons Center (private communication).